Springer

Acta Mechanica Sinica

CrossMark click for updates

• RESEARCH PAPER •

Acta Mech. Sin., Vol. 41, 423221 (2025)
https://doi.org/10.1007/s10409-024-23221-x

Mechanical manipulation of the transient negative capacitance effect in resistor-ferroelectric capacitor circuit

Qian He[1,2,3], Weijin Chen[1,2,3,4*], Xin Luo[1,2,3], and Yue Zheng[1,2,3]

[1] *Guangdong Provincial Key Laboratory of Magnetoelectric Physics and Devices, School of Physics, Sun Yat-sen University, Guangzhou 510275, China;*

[2] *State Key Laboratory of Optoelectronic Materials and Technologies, School of Physics, Sun Yat-sen University, Guangzhou 510275, China;*

[3] *Centre for Physical Mechanics and Biophysics, School of Physics, Sun Yat-sen University, Guangzhou 510275, China;*

[4] *School of Materials, Sun Yat-sen University, Shenzhen 518107, China*

Received May 13, 2024; accepted June 11, 2024; published online August 2, 2024

Transient negative capacitance (NC), as an available dynamic charge effect achieved in resistor-ferroelectric capacitor (R-FEC) circuits, has triggered a series of theoretical and experimental works focusing on its physical mechanism and device application. Here, we analytically derived the effects of different mechanical conditions on the transient NC behaviors in the R-FEC circuit based on the phenomenological model. It shows that the ferroelectric capacitor can exhibit either NC (i.e., "single NC" and "double NC") or positive capacitance, depending on the mechanical condition and temperature. Further numerical calculations show that the voltage drop caused by NC can be effectively controlled by temperature, applied stress, or strain. The relationship between NC voltage drop and system configurations including external resistance, dynamical coefficient of polarization, and input voltage are presented, showing diverse strategies to manipulate the NC effect. These results provide theoretical guidelines for rational design and efficient control of NC-related electronic devices.

Ferroelectric, Transient negative capacitance, Mechanical manipulation

Citation: Q. He, W. Chen, X. Luo, and Y. Zheng, Mechanical manipulation of the transient negative capacitance effect in resistor-ferroelectric capacitor circuit, Acta Mech. Sin. 41, 423221 (2025), https://doi.org/10.1007/s10409-024-23221-x

1. Introduction

With the rapid development of transistor technology and integration process, the size of microprocessors has been continuously decreasing to achieve high integration and maintain Moore's law [1,2]. Under such a development trend, the integrated circuit is facing increasing challenges due to the fundamental limit of power dissipation of a transistor known as Boltzmann tyranny [3,4]. In the past decade, ferroelectric negative capacitance (NC) has received intensive attention as a potential strategy to overcome the fundamental Boltzmann limit [5-18]. With a ferroelectric layer integrated into the field-effect transistor (FET) to form an NC FET, one can amplify the surface potential in the vicinity of the channel and realize a small sub-threshold swing (SS) (< 60 mV/dec) to reduce the device's power consumption [5].

One can notice two types of NC effects of ferroelectric capacitors [19-37]. One is the steady-state NC that is usually observed in ferroelectric-dielectric heterostructures [16,19]. The key for the occurring of steady-state NC is that the dielectric layer's energy contribution drives the heterostructure to maintain a non-polar state in which the local stiffness of the ferroelectric layer is negative [38]. The second type of NC effect is the transient NC that is usually observed in resistor-ferroelectric capacitor (R-FEC) circuits [14,20]. Manifested itself with a decrease (increasing) of voltage across the ferroelectric capacitor while charging (discharging), the transient NC originates from the mismatch between the screening charge accumulating rate and the polarization switching rate in the ferroelectric capacitor

*Corresponding author. E-mail address: chenweijin@mail.sysu.edu.cn (Weijin Chen)
Executive Editor: Xiaoding Wei

[21]. Compared with the steady-state NC effect, the transient NC would only appear and cause a voltage amplification during transient polarization switching [38], and its instability and hysteretic feature are considered as drawbacks in developing energy-efficient electronic devices. Despite this, the transient NC effect holds promise in the design of novel electronic devices and is a useful probe to explore the fundamental physics of ferroelectricity, hence it has recently received extensive technological and scientific interest. To maximize its possibilities, clear physical and theoretical descriptions on the ferroelectric transient NC effect are necessary. While it is well known that the free energy landscape of ferroelectric is sensitive to mechanical conditions, at present how the ferroelectric transient NC effect would be affected by the mechanical conditions remains unclear.

In this work, we investigate the effects of different mechanical conditions on the transient NC behaviors in the R-FEC circuit based on phenomenological model to present the universal relationship between different NC behaviors and the free energy landscape of different mechanical loadings. The temperature-stress and temperature-strain phase diagrams are analytically derived to show the mechanical manipulation of ferroelectric transient NC effect. The ferroelectric capacitor is found to exhibit either NC (including "single NC" and "double NC") or positive capacitance, due to the different free energy landscapes of the ferroelectric capacitor modulated by the mechanical condition and temperature. Based on Kirchhoff's law and the time-dependent Ginzburg-Landau (TDGL) equation, we calculate the voltage drop caused by NC effect as a function of temperature, applied stress, applied strain, external resistance, dynamical coefficient of polarization, and input voltage. Our study clearly indicates the potential of mechanically controlling the transient NC behaviors in the R-FEC circuit.

2. Thermodynamic framework

To theoretically study the ferroelectric transient NC effect and its controllability by mechanical conditions, we model an R-FEC circuit consisting of an external resistance R, a ferroelectric capacitor C_{FE}, and a voltage source with input voltage V_{in}, as shown schematically in Fig. 1. In this circuit, the current is governed by Kirchhoff's law:

$$RA\frac{\partial Q_{\mathrm{free}}}{\partial t} = V_{\mathrm{in}} - V_{\mathrm{FE}}, \tag{1}$$

where A is the sectional area of the capacitor, $\frac{\partial Q_{\mathrm{free}}}{\partial t}$ is the displacement current density, Q_{free} is the free charge density, and V_{FE} is the voltage across the ferroelectric capacitor C_{FE}. To clearly demonstrate the variation of the free energy landscape and its effects on NC behaviors under different mechanical conditions, we choose the uniaxial ferroelectric model for simplification, which means the polarization has only one component and should cross the energy barrier of zero-polarization while switching. The free energy landscape of the ferroelectric capacitor is described by a sixth-order Landau-type polynomial,

$$F = \frac{1}{2}\alpha_0(T - T_C)P^2 + \frac{1}{4}\beta P^4 + \frac{1}{6}\delta P^6 - E_{\mathrm{FE}}P, \tag{2}$$

where P is the spontaneous polarization, E is the electric field, α_0, β and δ are the Landau coefficients, and T_C is the Curie temperature. The evolution of spontaneous polarization obeys the TDGL equation, as the following form [39-43]:

$$\gamma\frac{\partial P}{\partial t} = -\frac{\delta F}{\delta P}, \tag{3}$$

where γ is the dynamical coefficient, and t is the time. The electrostatic equation of the screening charge of the capacitor is written as [39,44-46]

$$Q_{\mathrm{free}} = \varepsilon_{\mathrm{b}}E_{\mathrm{FE}} + P, \tag{4}$$

where ε_{b} is the background dielectric constant and E_{FE} is the electric field across the capacitor.

Chang et al. [21] theoretically demonstrated that the physical origin of the transient NC in R-FEC circuit is the mismatch between the screening charge accumulating rate and the polarization switching rate, which can be written as

$$\frac{\partial V_{\mathrm{FE}}}{\partial t} = \frac{t_{\mathrm{FE}}}{\varepsilon_{\mathrm{b}}}\left(\frac{\partial Q_{\mathrm{free}}}{\partial t} - \frac{\partial P}{\partial t}\right), \tag{5}$$

where t_{FE} is the thickness of the capacitor. When $\frac{\partial Q_{\mathrm{free}}}{\partial t} < \frac{\partial P}{\partial t}$ is satisfied, NC effect appears. When the polarization switching rate is not too large, the transient NC effect region of an R-FEC circuit can be considered a direct mapping of the negative curvature in the free energy profile under equilibrium (i.e., without the electric field) [21]. Based on this model, we further consider a first-order ferroelectric capacitor, which means the Landau coefficients are satisfying $\delta > 0$ and $\beta < 0$. As the temperature decreases from high above Curie temperature to far below Curie temperature, the free energy landscape of the ferroelectric evolves from single well, to triple well, and finally to double well. This results in none, two, and one INC region(s), corresponding to none, double NC effect, and single NC effect as shown in Fig. 1b. Since there have been several works proving that mechanical conditions can significantly change the properties of the ferroelectrics like transition temperatures and even the order of phase transition [23,47-50], in the following sections we explore how the mechanical conditions would affect the transient NC effects.

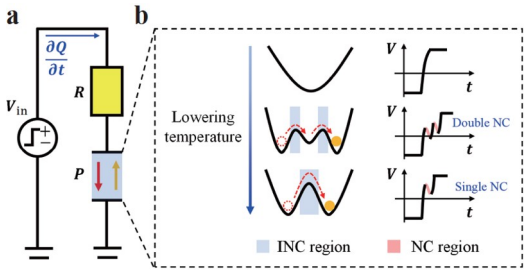

Figure 1 **a** Schematic of the model R-FEC circuit. **b** Schematic of various voltage responses of the ferroelectric capacitor during switching in the R-FEC circuit. "INC" is the abbreviation for intrinsic negative curvature.

3. Mechanical manipulation of transient NC effect

3.1 Multiple NC behaviors regulated by applied stress

Based on the first law of thermodynamics and to consider the coupling between polarization and stress, the capacitor's free energy should be replaced by the Gibbs free energy, following

$$G=\frac{1}{2}\alpha_0(T-T_C)P^2+\frac{1}{4}\beta P^4+\frac{1}{6}\delta P^6-QP^2\sigma -\frac{1}{2}s\sigma^2-E_{\mathrm{FE}}P, \tag{6}$$

where σ is stress, s is the elastic compliance coefficient, and Q is the electrostrictive coefficient. Considering the equilibrium condition, the electric field E_{FE} is set to zero. By combining the coefficients of the second-order term, we can obtain the modified transition temperature $T_C^{'}=T_C+2\sigma Q/\alpha_0$. Assuming $\delta>0$ and $\alpha_0>0$, here we discuss the modulation effects of applied stress and temperature on the INC regions or NC behaviors in two different situations: $\beta>0$ or $\beta<0$.

For the case $\beta<0$, the ferroelectric phase transition is of first-order feature, and the second-order partial derivative of the Gibbs free energy gives the curvature of the free energy curve, following

$$\frac{\partial^2 G}{\partial P^2}=\alpha_0(T-T_C)-2Q\sigma+3\beta P^2+5\delta P^4. \tag{7}$$

One can solve the equation $\partial^2 G/\partial P^2=0$ and derive three different situations in which the system may have different INC regions and exhibit various NC behaviors, as shown in Fig. 2a. For the condition σ and T satisfying $T<(2Q/\alpha_0)\sigma+0.45\beta^2/(\alpha_0\delta)+T_C$ and $(2Q/\alpha_0)\sigma+T_C<T$, the ferroelectric capacitor would exhibit a double NC during the polarization switching process. For σ and T satisfying $T\le(2Q/\alpha_0)\sigma+T_C$, the system would have only one INC region and exhibit a single NC effect. Moreover, if $T\geqslant(2Q/\alpha_0)\sigma+0.45\beta^2/(\alpha_0\delta)+T_C$, the system would not show NC effect.

For the case $\beta>0$, the ferroelectric phase transition is of second-order feature and the solution for double NC vanishes. For σ and T satisfying $T\le(2Q/\alpha_0)\sigma+T_C$, the system would exhibit a single NC effect, and for the condition $T>(2Q/\alpha_0)\sigma+T_C$, the system would not show NC effect, as shown in Fig. 2b.

Moreover, the temperature evolution of G-P curves is calculated for first-order ferroelectric under constant applied stress, as shown in Fig. 2c. As we can see, when increasing the temperature, the free energy landscape of a first-order ferroelectric transforms from double-well to triple-well and then to single-well, corresponding to single, double NC effect, and none NC effect in an R-FEC circuit.

The above derivation demonstrates that controlling the ambient temperature and external stress of the ferroelectric capacitor can effectively regulate the transient NC behaviors of the R-FEC circuit. Based on the classic sixth-order Landau potentials for conventional perovskite ferroelectrics $BaTiO_3$ (BTO) and $PbTiO_3$ (PTO) [47], we use a numerical method to simulate the NC effects in the R-FEC circuit, as shown in Fig. 3 (stress-free condition). During the simulation, an input voltage step varying from +3 V to −3 V is used to switch the polarization in our simulations. As we can see in Fig. 3, the voltage drop caused by the NC of both ferroelectric capacitors is nonlinearly modulated by temperature in stress-free condition and there is a sudden change in voltage drop at the transition point from the single NC region to the double NC region. Comparing the results of BTO and PTO, one can also see that the voltage drop caused by the NC of the PTO capacitor is generally more significant than that of the BTO capacitors. Moreover, the double NC region of PTO capacitor has a wider temperature range than that of BTO capacitor.

The temperature-stress phase diagrams showing various NC behaviors of the R-FEC circuit are further calculated based on the BTO and PTO Landau coefficients and shown in Fig. 4. The three NC behaviors are marked by three colors and the voltage drops caused by the NC are displayed through contour lines. From Fig. 4, it shows that a higher positive stress or a lower temperature will increase the magnitude of the voltage drop. Comparing the results of the BTO and PTO capacitors, one can also see that the NC boundaries (i.e., that between the "single NC" and the "double NC" region and that between the "no NC" region and the "double NC" region) of the BTO capacitor is more sensitive to the applied stress than those of the PTO capacitor, due to the larger value of $2Q/\alpha_0$. Moreover, the temperature range of double NC region of the BTO capacitor decreases with the increase of the applied stress, due to the temperature dependence of the fourth-order Landau parameter of the bulk BTO.

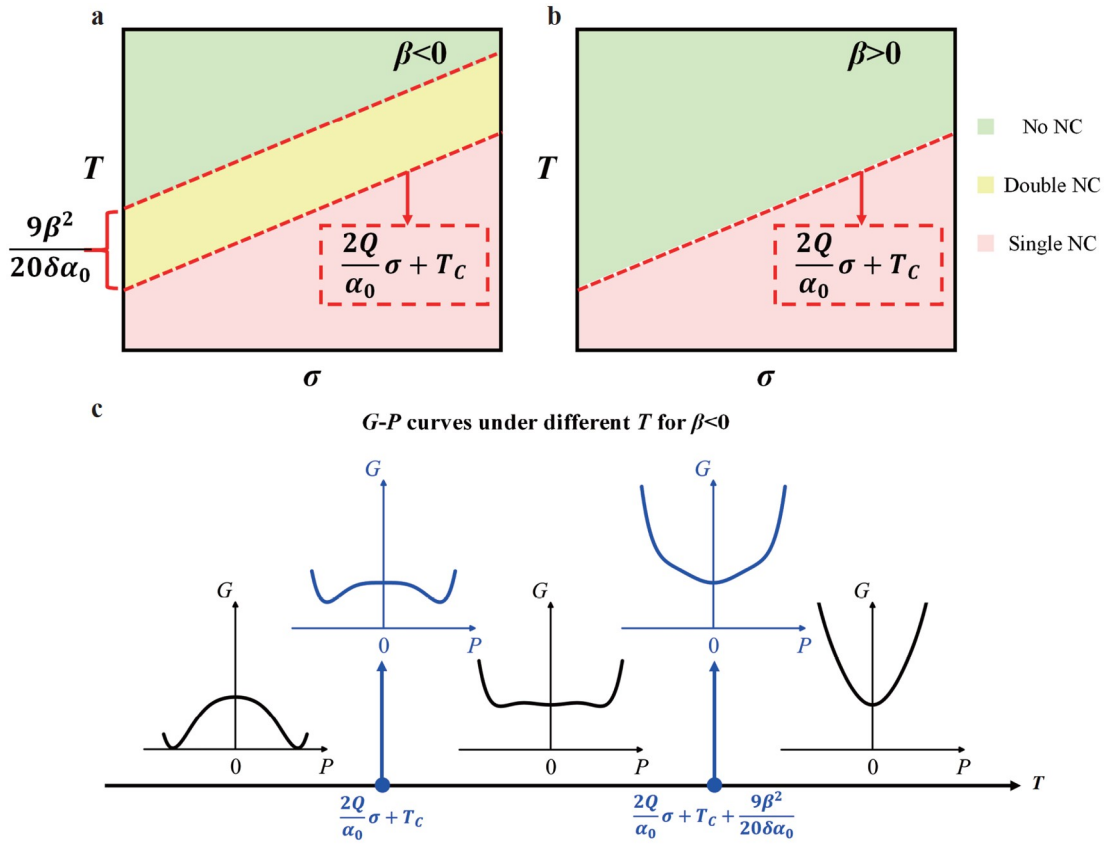

Figure 2 Temperature-stress phase diagram depicting various transient NC effects. **a** The case $\beta < 0$. **b** The case $\beta > 0$. **c** The temperature evolution of *G*-*P* curves for first-order ferroelectric under constant applied stress.

3.2 Multiple NC behaviors regulated by applied strain

Considering the ferroelectric is in strained, the electrical Gibbs function G_2 should be chosen as the system's thermodynamic potential, which can be derived from the Legendre transformation of the Gibbs free energy G, as

$$G_2 = G + \sigma\varepsilon = \frac{1}{2}\alpha_0(T - T_C)P^2 + \frac{1}{4}\beta P^4 + \frac{1}{6}\delta P^6 - QP^2\sigma - \frac{1}{2}s\sigma^2 + \sigma\varepsilon - E_{\mathrm{FE}}P, \tag{8}$$

where ε is strain. Substituting $\frac{\partial G}{\partial \sigma} = -QP^2 - s\sigma = -\varepsilon$ into G_2 and setting the electric field E_{FE} to zero, the electrical Gibbs function can be rewritten as

$$G_2 = \frac{1}{2}\alpha_0(T - T_C)P^2 + \frac{1}{4}\beta P^4 + \frac{1}{6}\delta P^6 - QP^2\left(\frac{\varepsilon - QP^2}{s}\right) - \frac{1}{2}s\left(\frac{\varepsilon - QP^2}{s}\right)^2 + \left(\frac{\varepsilon - QP^2}{s}\right)\varepsilon. \tag{9}$$

Combining the coefficients of the second-order and fourth-order terms, we have the following form of the electrical Gibbs function:

$$G_2 = \left[\frac{\alpha_0(T - T_C)}{2} - \frac{Q\varepsilon}{s}\right]P^2 + \left(\frac{\beta}{4} + \frac{Q^2}{2s}\right)P^4 + \frac{1}{6}\delta P^6 + \frac{\varepsilon^2}{2s}. \tag{10}$$

Rewriting the second-order and fourth-order terms, we have

$$G_2 = \frac{1}{2}\alpha_0\left(T - T_C'\right)P^2 + \frac{1}{4}\beta' P^4 + \frac{1}{6}\delta P^6 + \frac{\varepsilon^2}{2s}, \tag{11}$$

with $T_C' = T_C + \frac{2Q\varepsilon}{s\alpha_0}$, $\beta' = \beta + 2Q^2/s$. From Eq. (11), one can see that the strain modulates the transition temperature T_C of the ferroelectrics, and it can even change the order of phase transition. Assuming the elastic compliance coefficient s to be positive, the strain effect can increase β from negative to positive by $\beta' = \beta + 2Q^2/s$, leading to a change of phase transition order from first-order type to second-order type. The curvature of the electrical Gibbs function curve can be derived from

$$\frac{\partial^2 G_2}{\partial P^2} = \alpha_0(T - T_C) - \frac{2Q\varepsilon}{s} + \left(3\beta + \frac{6Q^2}{s}\right)P^2 + 5\delta P^4. \tag{12}$$

According to Eq. (12), for the case that $\beta' < 0$, if ε and T satisfy $T \le [2Q/(\alpha_0 s)]\varepsilon + T_C$, the system would exhibit a single NC effect. For condition that $T > [2Q/(\alpha_0 s)]\varepsilon + T_C$ and $\left(9\beta^2 s^2 + 36\beta s Q^2 + 36Q^4\right)/\left(20\alpha_0\delta s^2\right) + [2Q/(\alpha_0 s)]\varepsilon + T_C > T$, the system would exhibit double NC

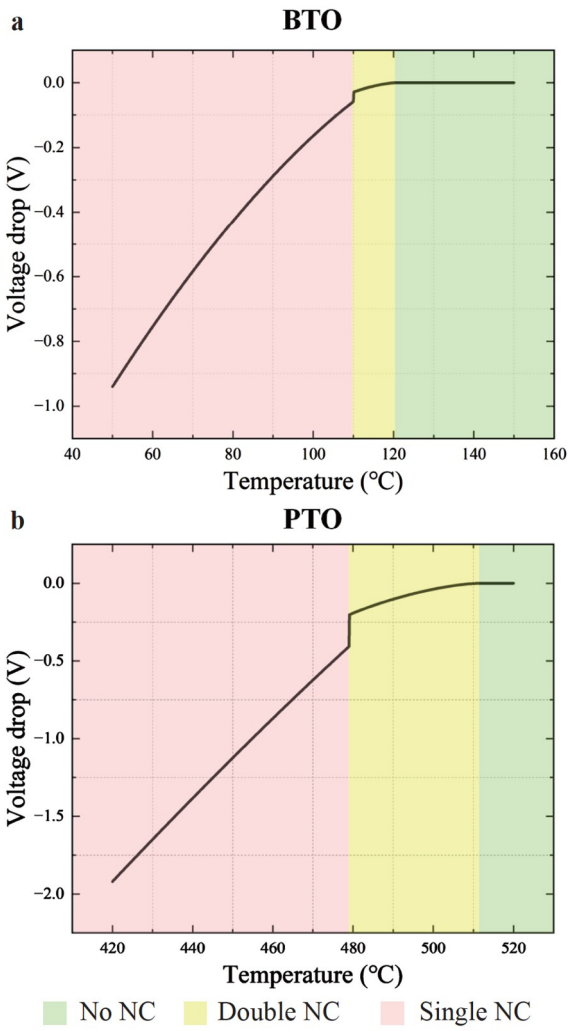

Figure 3 NC behaviors of the R-FEC circuit with a stress-free ferroelectric capacitor. **a** Voltage drop-temperature relation curve calculated with BTO's Landau coefficients. **b** Voltage drop-temperature relation curve calculated with PTO's Landau coefficients.

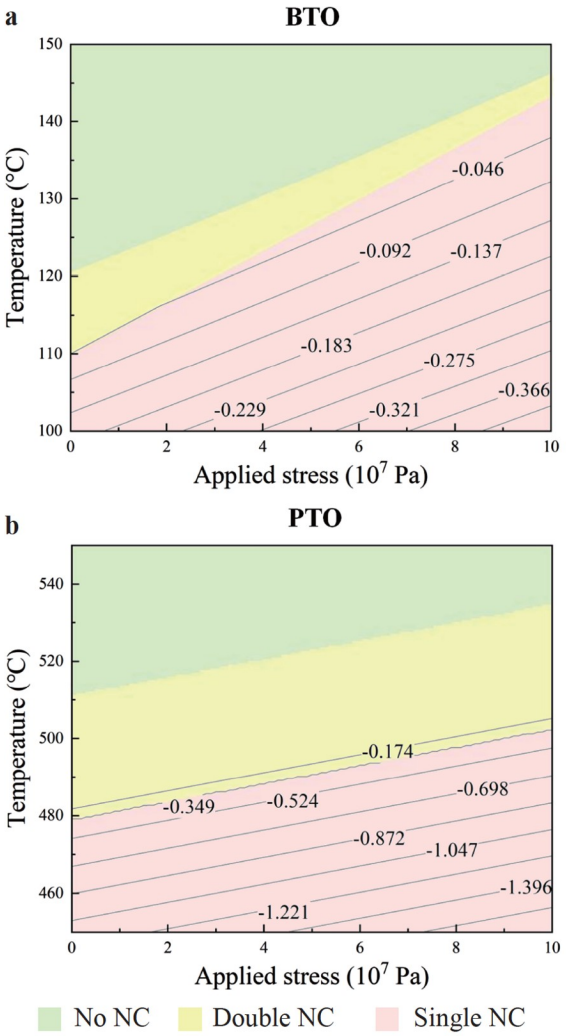

Figure 4 Calculated temperature-stress phase diagram of various NC behaviors in the R-FEC circuit using the perovskite ferroelectrics' coefficients. **a** Phase diagram calculated by BTO's coefficients. **b** Phase diagram calculated by PTO's coefficients.

effect during polarization switching. When the system satisfies $\left(9\beta^2 s^2+36\beta s Q^2+36Q^4\right)/\left(20\alpha_0\delta s^2\right)+[2Q/(\alpha_0 s)]\varepsilon+T_C\le T$, there are no NC effects during polarization switching. The temperature-strain phase diagram is shown in Fig. 5a.

For the case that $\beta'>0$, the change of temperature and applied strain would only induce the transformation between "single NC" state and "no NC" state of the system. For condition satisfying $T\le[2Q/(\alpha_0 s)]\varepsilon+T_C$, the system would exhibit a single NC effect, and for $T>[2Q/(\alpha_0 s)]\varepsilon+T_C$, there will be no NC effects, as shown in Fig. 5b.

The temperature evolution of G_2-P curves is also calculated for first-order ferroelectric under constant applied strain, as shown in Fig. 5c.

To numerically consider the effects of temperature and applied strain on the NC behavior and voltage drop of the ferroelectric capacitor during polarization switching, we further use the Landau coefficients of BTO and PTO to calculate the temperature-strain phase diagram with contours of voltage drop, as shown in Fig. 6. Here in the simulation, biaxial strains are applied along x and y directions, given by $\frac{\partial G}{\partial \sigma_{x(y)}}=-\varepsilon$. The expression of the electrical Gibbs function and the simulation parameters can be found in Appendix. Comparing the temperature-strain phase diagrams shown in Fig. 6 and the temperature-stress phase diagram shown in Fig. 4, one can see that the applied strain significantly depresses the double NC region of both the BTO and PTO capacitors. Moreover, the specific Landau potential of PTO results in an order change of phase transition from first-order to second-order due to the clamped effect of the applied strain,

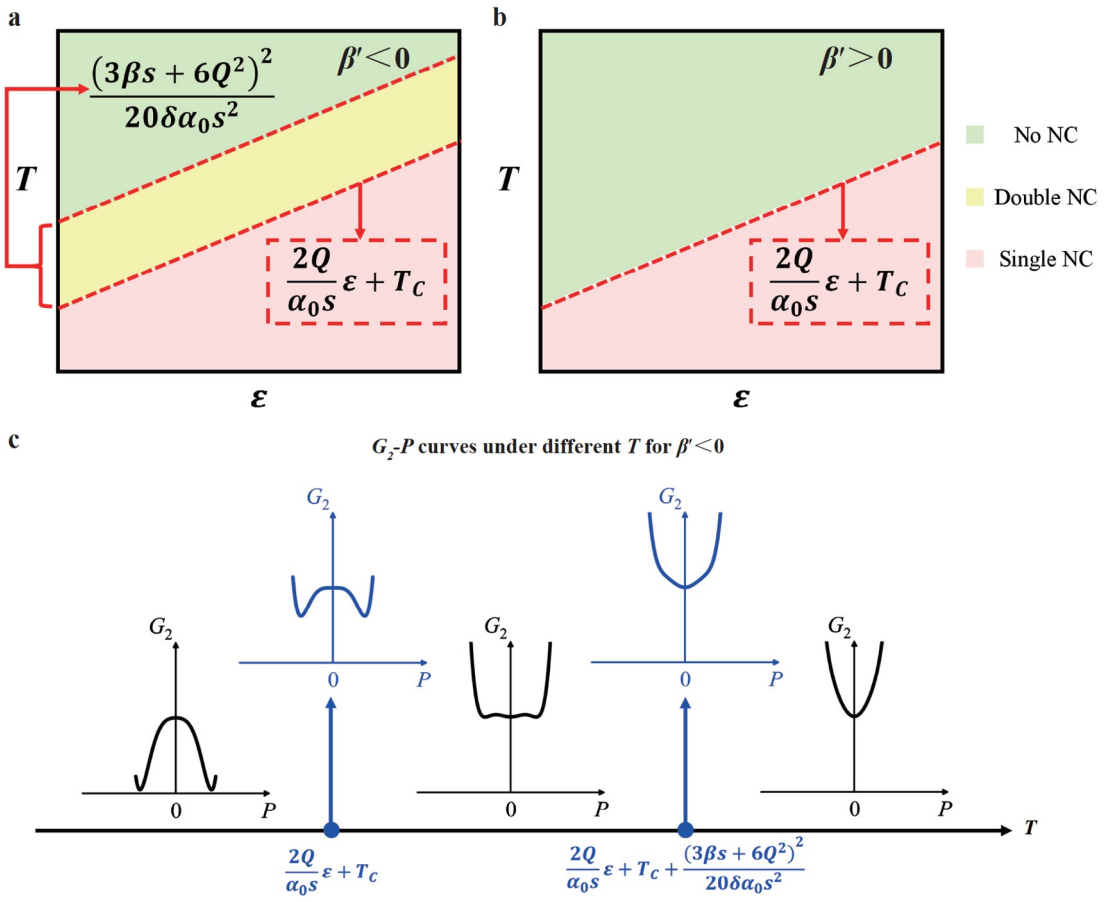

Figure 5 Temperature-strain phase diagram containing various transient NC effects. **a** The case $\beta' < 0$. **b** The case $\beta' > 0$. **c** The temperature evolution of G_2-P curves under constant applied strain.

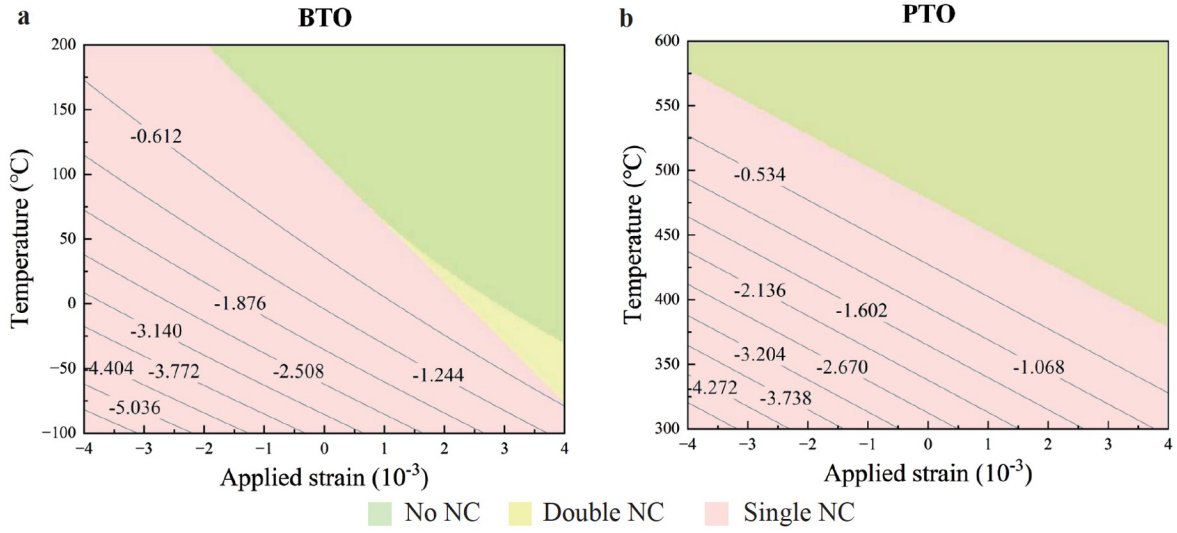

Figure 6 Calculated temperature-strain phase diagram of various NC behaviors in the R-FEC circuit using the perovskite ferroelectrics' coefficients. **a** Phase diagram calculated by BTO's coefficients. **b** Phase diagram calculated by PTO's coefficients.

leading to the vanishing of double NC region. From Fig. 6, it can be also seen that alower negative strain or a lower temperature would increase the magnitude of the voltage drop.

4. Additional influencing factors

The above results have proven that temperature, stress, and strain can effectively control the NC behaviors of R-FEC

circuit. To further explore the factors that affect the NC behaviors of R-FEC circuit, we adopt different values of external resistance R or dynamical coefficient γ to calculate the voltage drop during polarization switching, as shown in Fig. 7. As we can see, the external resistance and dynamical coefficient can significantly affect the voltage drop during transient NC progress. A larger resistance or a smaller dynamical coefficient can nonlinearly increase the magnitude of the voltage drop. Moreover, both the external resistance and dynamical coefficient can manipulate the relaxation time of the polarization switching. An R-FEC circuit with larger external resistance or larger dynamical coefficient would significantly increase the polarization switching time.

To find out the relationship between the voltage drop of NC and input voltage, we further calculate the transient NC behaviors under different input voltages from 2 V to 5 V, as shown in Fig. 8a. The relative polarization evolution curves are shown in Fig. 8b. Among the four different input voltage conditions in Fig. 8, the polarization under the lowest input voltage condition (green line) does not complete switching and hence exhibits no NC effect in the circuit. The other three conditions with their input voltage larger than a critical value finish polarization switching and gain a voltage drop of −5.33 V. Hence, we can see that the magnitude of the input voltage affects the polarization switching process of the ferroelectric capacitor and there is a critical voltage threshold above which the polarization can be completely reversed. When the input voltage exceeds the critical value, in other words, the polarization completes switching through the INC region of the free energy curve, the voltage drop of NC would not change with the enlarging input voltage. The above calculations inspire us to design the intrinsic free energy curve of the ferroelectric or the circuit's configurations to efficiently control the NC effect.

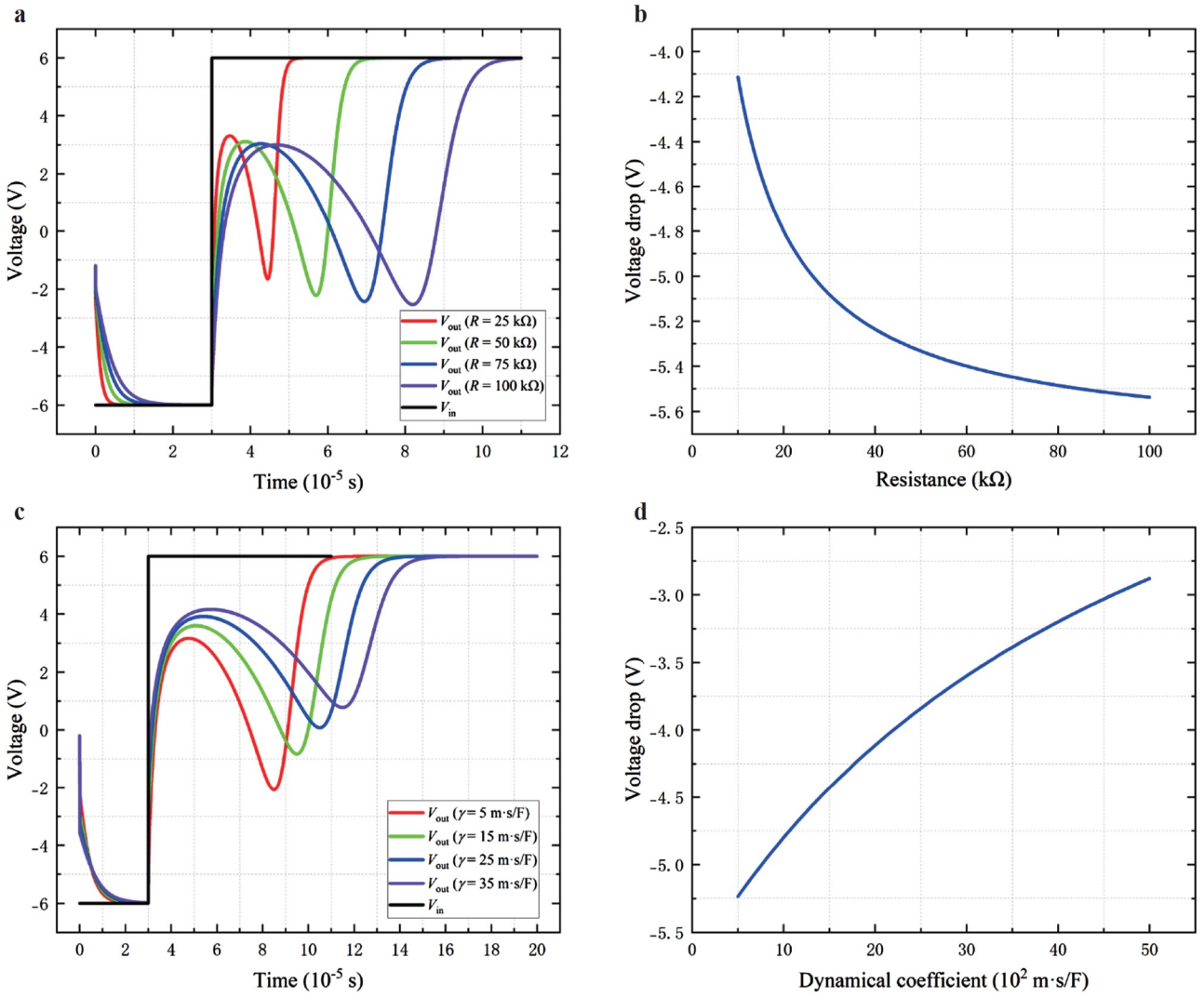

Figure 7 NC behaviors of the R-FEC circuit with different circuit configurations. **a** NC behaviors of the R-FEC circuit with different external resistance. **b** Voltage drop-resistance relation curve. **c** NC behaviors of the R-FEC circuit with different dynamical coefficients. **d** Voltage drop-dynamical coefficient relation curve.

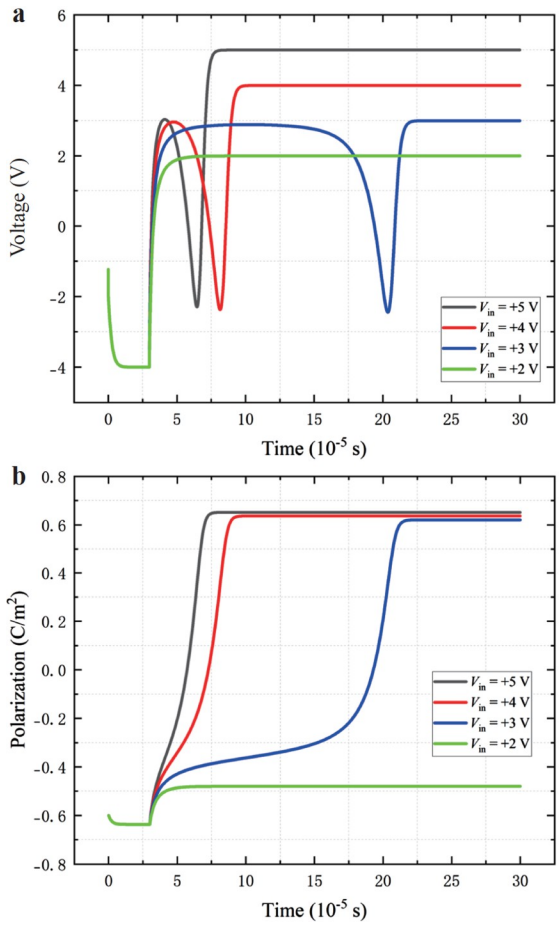

Figure 8 **a** NC behaviors of the R-FEC circuit under different input voltages. **b** The evolution of polarization under different input voltages.

5. Conclusions

In conclusion, we have analytically derived the effects of different mechanical conditions on the transient NC behaviors in the R-FEC circuit. It shows that with a first-order ferroelectric capacitor in the R-FEC circuit, the temperature and applied stress or strain can effectively manipulate the NC behaviors, leading to transformation between "no NC", "single NC", and "double NC" states. Based on the Landau coefficients of perovskite ferroelectrics, the numerical calculations show that lower temperature, larger applied stress, or larger compressive strain can significantly increase the voltage drop caused by the NC effect. Moreover, we reveal the nonlinear control of the ferroelectric dynamical coefficient and external resistance on the voltage drop of transient NC. These results provide theoretical guidelines for rational design and efficient control of NC-related electronic devices. The relationship between free energy landscape and multiple transient NC effects inspires us to design the polarization switching process in the R-FEC circuits to gain different NC effects. For example, by doping, using new-type multi-well ferroelectric materials, and designing compensated multi-domain switching processes, we can control the height and number of barriers that polarization switching needs to cross and gain different transient NC effects. Moreover, the strategy of mechanically reducing the polarization switching barrier enables high-speed digital electronic devices based on transient NC effects to operate at low voltage and high frequency, and the mechanically manipulable double NC effect can be applied in waveform modulators which convert rectangular pulses into wavy-shaped pulses.

Appendix

In Sect. 3.2, we calculate the effect of strain on the NC behaviors of the R-FEC circuit based on the specific Landau coefficients of BTO and PTO. The electrical Gibbs function of the ferroelectric capacitor has the form:

$$G_2 = \left[\frac{\alpha_0(T-T_C)}{2} - \varepsilon\frac{2Q_{12}}{s_{11}+s_{12}}\right]P^2 + \left(\frac{\beta}{4} + \frac{Q_{12}^2}{s_{11}+s_{12}}\right)P^4 + \delta P^6 + \frac{\varepsilon^2}{s_{11}+s_{12}} - E_{\mathrm{FE}}P,$$

where ε is the biaxial strain applied along x and y directions that are perpendicular to the polarization.

Values of the parameters in the simulations are shown in Table A1.

Table A1 Values of the parameters used in the simulation of transient NC effects in the R-FEC circuit[a)]

Parameter	Value (BTO/PTO)
a (10^5 C^{-2} m^2 N)	$3.3(T-110)/3.8(T-479)$
b (10^7 C^{-4} m^6 N)	$0.36(T-175)/-7.3$
c (10^9 C^{-6} m^{10} N)	6.6/0.26
s (10^{-12})	8.3/8.0
Q	0.11/0.089
R (kΩ)	50
ε_b (10^{-12} m^{-1})	8.85
A (10^{-12} m^2)	2500
γ (m sec F^{-1})	200
V_{in} (V)	±3

a) Specifically, $a = \frac{1}{2}\alpha_0(T-T_C)$, $b = \frac{1}{4}\beta$ and $c = \frac{\delta}{6}$ for abbreviations.

Conflict of interest *On behalf of all authors, the corresponding author states that there is no conflict of interest.*

Author contributions ***Qian He:*** *Formal analysis, Investigation, Validation, Writing – original draft, Writing – review & editing.* ***Weijin Chen:*** *Conceptualization, Data curation, Funding acquisition, Software, Supervision, Writing – review & editing.* ***Xin Luo:*** *Funding acquisition, Project administration, Supervision.* ***Yue Zheng:*** *Funding acquisition, Project administration, Resources, Supervision, Writing – review & editing.*

Acknowledgements *This work was supported by the National Natural*

Science Foundation of China (Grants Nos. 12222214, 12132020, 12002400, and 12172386), by Guangdong Provincial Key Laboratory of Magnetoelectric Physics and Devices (Grant No. 2022B1212010008), by the National Natural Science Foundation of Guangdong Province (Grant No. 2021B1515020021) and by the Shenzhen Science and Techonlogy Program (Grant Nos. 20220619300001 and 20220818181805001).

1 G. E. Moore, Cramming more components onto integrated circuits, Proc. IEEE **86**, 82 (1998).
2 M. M. Waldrop, The chips are down for Moore's law, Nature **530**, 144 (2016).
3 V. V. Zhirnov, and R. K. Cavin, Negative capacitance to the rescue? Nat. Nanotech. **3**, 77 (2008).
4 J. D. Meindl, Q. Chen, and J. A. Davis, Limits on silicon nanoelectronics for terascale integration, Science **293**, 2044 (2001).
5 S. Salahuddin, and S. Datta, Use of negative capacitance to provide voltage amplification for low power nanoscale devices, Nano Lett. **8**, 405 (2008).
6 M. Hoffmann, F. P. G. Fengler, M. Herzig, T. Mittmann, B. Max, U. Schroeder, R. Negrea, P. Lucian, S. Slesazeck, and T. Mikolajick, Unveiling the double-well energy landscape in a ferroelectric layer, Nature **565**, 464 (2019).
7 S. Smith, K. Chatterjee, and S. Salahuddin, Multidomain phase-field modeling of negative capacitance switching transients, IEEE Trans. Electron Devices **65**, 295 (2018).
8 H. W. Park, J. Roh, Y. B. Lee, and C. S. Hwang, Modeling of negative capacitance in ferroelectric thin films, Adv. Mater. **31**, 1805266 (2019).
9 K. Majumdar, S. Datta, and S. P. Rao, Revisiting the theory of ferroelectric negative capacitance, IEEE Trans. Electron Devices **63**, 2043 (2016).
10 M. Hoffmann, A. I. Khan, C. Serrao, Z. Lu, S. Salahuddin, M. Pešić, S. Slesazeck, U. Schroeder, and T. Mikolajick, Ferroelectric negative capacitance domain dynamics, J. Appl. Phys. **123**, 184101 (2018).
11 A. Islam Khan, D. Bhowmik, P. Yu, S. Joo Kim, X. Pan, R. Ramesh, and S. Salahuddin, Experimental evidence of ferroelectric negative capacitance in nanoscale heterostructures, Appl. Phys. Lett. **99**, 113501 (2011).
12 W. Gao, A. Khan, X. Marti, C. Nelson, C. Serrao, J. Ravichandran, R. Ramesh, and S. Salahuddin, Room-temperature negative capacitance in a ferroelectric-dielectric superlattice heterostructure, Nano Lett. **14**, 5814 (2014).
13 D. J. R. Appleby, N. K. Ponon, K. S. K. Kwa, B. Zou, P. K. Petrov, T. Wang, N. M. Alford, and A. O'Neill, Experimental observation of negative capacitance in ferroelectrics at room temperature, Nano Lett. **14**, 3864 (2014).
14 A. I. Khan, K. Chatterjee, B. Wang, S. Drapcho, L. You, C. Serrao, S. R. Bakaul, R. Ramesh, and S. Salahuddin, Negative capacitance in a ferroelectric capacitor, Nat. Mater **14**, 182 (2015).
15 S. J. Song, Y. J. Kim, M. H. Park, Y. H. Lee, H. J. Kim, T. Moon, K. Do Kim, J. H. Choi, Z. Chen, A. Jiang, and C. S. Hwang, Alternative interpretations for decreasing voltage with increasing charge in ferroelectric capacitors, Sci. Rep. **6**, 20825 (2016).
16 P. Zubko, J. C. Wojdeł, M. Hadjimichael, S. Fernandez-Pena, A. Sené, I. Luk'yanchuk, J. M. Triscone, and J. Íñiguez, Negative capacitance in multidomain ferroelectric superlattices, Nature **534**, 524 (2016).
17 X. Liu, R. Liang, G. Gao, C. Pan, C. Jiang, Q. Xu, J. Luo, X. Zou, Z. Yang, L. Liao, and Z. L. Wang, MoS_2 negative-capacitance field-effect transistors with subthreshold swing below the physics limit, Adv. Mater. **30**, 1800932 (2018).
18 A. K. Yadav, K. X. Nguyen, Z. Hong, P. García-Fernández, P. Aguado-Puente, C. T. Nelson, S. Das, B. Prasad, D. Kwon, S. Cheema, A. I. Khan, C. Hu, J. Íñiguez, J. Junquera, L. Q. Chen, D. A. Muller, R. Ramesh, and S. Salahuddin, Spatially resolved steady-state negative capacitance, Nature **565**, 468 (2019).
19 S. C. Chang, U. E. Avci, D. E. Nikonov, and I. A. Young, A thermodynamic perspective of negative-capacitance field-effect transistors, IEEE J. Explor. Solid-State Comput. Devices Circuits **3**, 56 (2017).
20 M. Hoffmann, M. Pešić, K. Chatterjee, A. I. Khan, S. Salahuddin, S. Slesazeck, U. Schroeder, and T. Mikolajick, Direct observation of negative capacitance in polycrystalline ferroelectric HfO_2, Adv. Funct. Mater. **26**, 8643 (2016).
21 S. C. Chang, U. E. Avci, D. E. Nikonov, S. Manipatruni, and I. A. Young, Physical origin of transient negative capacitance in a ferroelectric capacitor, Phys. Rev. Appl. **9**, 014010 (2018).
22 M. Hoffmann, M. Pešić, S. Slesazeck, U. Schroeder, and T. Mikolajick, On the stabilization of ferroelectric negative capacitance in nanoscale devices, Nanoscale **10**, 10891 (2018).
23 C. Liu, and J. Wang, Strain engineering of ferroelectric negative capacitance in $PbZr_{(1-x)}Ti_xO_3$ thin films, Acta Mater. **206**, 116607 (2021).
24 Y. Zhang, X. Sun, J. Chai, H. Xu, X. Ma, J. Xiang, K. Han, X. Wang, W. Wang, and T. Ye, Thermodynamic driving force of transient negative capacitance of ferroelectric capacitors, Appl. Phys. Lett. **119**, 022901 (2021).
25 E. A. Eliseev, M. E. Yelisieiev, S. V. Kalinin, and A. N. Morozovska, Observability of negative capacitance of a ferroelectric film: Theoretical predictions, Phys. Rev. B **105**, 174110 (2022).
26 A. N. Morozovska, E. A. Eliseev, S. Cherifi-Hertel, D. R. Evans, and R. Hertel, Electric field control of labyrinth domain structures in core-shell ferroelectric nanoparticles, Phys. Rev. B **106**, 144104 (2022).
27 Y. Dong, D. Chen, N. Zhong, J. Liu, C. Duan, and X. Li, Systematic interpretation of time effect on negative capacitance of ferroelectrics based on electrostatics and charge dynamics, IEEE Trans. Electron Devices **69**, 5913 (2022).
28 H. W. Park, M. Oh, and C. S. Hwang, Negative capacitance from the inhomogenous stray field in a ferroelectric-dielectric structure, Adv. Funct. Mater. **32**, 2200389 (2022).
29 R. Chen, and Y. Lu, Negative capacitance field effect transistors based on Van der Waals 2D materials, Small (2023).
30 L. Liu, L. Lei, X. Lu, Y. Xia, Z. Wu, and F. Huang, Direct measurement of negative capacitance in ferroelectric/semiconductor heterostructures, ACS Appl. Mater. Interfaces **15**, 10175 (2023).
31 H. W. Park, M. Oh, I. S. Lee, S. Byun, Y. H. Jang, Y. B. Lee, B. Y. Kim, S. H. Lee, S. K. Ryoo, D. Shim, J. H. Lee, H. Kim, K. D. Kim, and C. S. Hwang, Double S-shaped polarization-voltage curve and negative capacitance from Al_2O_3-$Hf_{0.5}Zr_{0.5}O_2$-Al_2O_3 triple-layer structure, Adv. Funct. Mater. **33**, 2206637 (2023).
32 Y. Luo, Z. Wang, Y. Chen, M. Qin, Z. Fan, M. Zeng, G. Zhou, X. Lu, X. Gao, D. Chen, and J. M. Liu, Strain tuning of negative capacitance in ferroelectric $KNbO_3$ thin films, ACS Appl. Mater. Interfaces **15**, 16902 (2023).
33 X. Huang, J. Tao, Z. Tang, L. Liu, F. Zhang, W. Chen, and Y. Zheng, Phase field study on the flexoelectric response of dielectric–ferroelectric multilayers, J. Appl. Phys. **134**, 014101 (2023).
34 D. Daw, H. Bouzid, M. Jung, D. Suh, C. Biswas, and Y. Hee Lee, Ultrafast negative capacitance transition for 2D ferroelectric MoS_2 /graphene transistor, Adv. Mater. **36**, 2304338 (2024).
35 A. N. Morozovska, E. A. Eliseev, O. A. Kovalenko, and D. R. Evans, Influence of chemical strains on the electrocaloric response, polarization morphology, tetragonality, and negative-capacitance effect of ferroelectric core-shell nanorods and nanowires, Phys. Rev. Appl. **21**, 054035 (2024).
36 S. S. Cheema, N. Shanker, S. L. Hsu, J. Schaadt, N. M. Ellis, M. Cook, R. Rastogi, R. C. N. Pilawa-Podgurski, J. Ciston, M. Mohamed, and S. Salahuddin, Giant energy storage and power density negative capacitance superlattices, Nature **629**, 803 (2024).
37 Y. Wu, H. Yang, Q. He, H. Jiang, W. Chen, C. Tan, Y. Zhang, and Y. Zheng, The investigation of neuromimetic dynamics in ferroelectrics via *in situ* TEM, Nano Lett. **24**, 7424 (2024).
38 J. Íñiguez, P. Zubko, I. Luk'yanchuk, and A. Cano, Ferroelectric negative capacitance, Nat. Rev. Mater. **4**, 243 (2019).

39 Y. Liu, X. Lou, M. Bibes, and B. Dkhil, Effect of a built-in electric field in asymmetric ferroelectric tunnel junctions, Phys. Rev. B **88**, 024106 (2013).
40 R. Kretschmer, and K. Binder, Surface effects on phase transitions in ferroelectrics and dipolar magnets, Phys. Rev. B **20**, 1065 (1979).
41 S. C. Chang, S. Manipatruni, D. E. Nikonov, and I. A. Young, Clocked domain wall logic using magnetoelectric effects, IEEE J. Explor. Solid-State Comput. Devices Circuits **2**, 1 (2016).
42 Y. Qi, and A. M. Rappe, Designing ferroelectric field-effect transistors based on the polarization-rotation effect for low operating voltage and fast switching, Phys. Rev. Appl. **4**, 044014 (2015).
43 G. Vizdrik, S. Ducharme, V. M. Fridkin, and S. G. Yudin, Kinetics of ferroelectric switching in ultrathin films, Phys. Rev. B **68**, 094113 (2003).
44 G. Gerra, A. K. Tagantsev, and N. Setter, Ferroelectricity in asymmetric metal-ferroelectric-metal heterostructures: A combined first-principles–phenomenological approach, Phys. Rev. Lett. **98**, 207601 (2007).
45 A. K. Tagantsev, G. Gerra, and N. Setter, Short-range and long-range contributions to the size effect in metal-ferroelectric-metal heterostructures, Phys. Rev. B **77**, 174111 (2008).
46 Y. Zheng, and C. H. Woo, Thermodynamic modeling of critical properties of ferroelectric superlattices in nano-scale, Appl. Phys. A **97**, 617 (2009).
47 N. A. Pertsev, A. G. Zembilgotov, and A. K. Tagantsev, Effect of mechanical boundary conditions on phase diagrams of epitaxial ferroelectric thin films, Phys. Rev. Lett. **80**, 1988 (1998).
48 W. J. Chen, Y. Zheng, B. Wang, D. C. Ma, and C. M. Wu, Misfit strain-temperature phase diagrams and domain stability of asymmetric ferroelectric capacitors: Thermodynamic calculation and phase-field simulation, J. Appl. Phys. **115**, 094101 (2014).
49 L. Chen, Phase-field method of phase transitions/domain structures in ferroelectric thin films: A review, J. Am. Ceram. Soc. **91**, 1835 (2008).
50 Y. Zheng, B. Wang, and C. H. Woo, Simulation of characteristics of phase transitions in ferroelectric thin films, Phys. Lett. A **368**, 117 (2007).

电阻-铁电电容器电路中瞬态负电容效应的力学调控研究

何乾, 陈伟津, 罗鑫, 郑跃

摘要 瞬态负电容效应作为一种在电阻-铁电电容器电路中实现的可用动态电荷效应, 已受到科研人员的广泛关注. 近年来, 已有许多研究者针对其物理机制与器件应用开展了一系列理论与实验研究. 本文通过解析推导研究了不同力学条件对电阻-铁电电容器电路中的瞬态负电容效应的影响, 结果显示在不同的力学与温度条件下, 一级铁电体电容器可以发生不同的负电容效应（包括单负电容与双负电容效应）以及不发生负电容效应. 数值模拟的结果表明, 较低的温度、较大的施加应力以及较大的压缩失配应变可以显著地增加负电容的电压降. 此外, 负电容电压降与不同的电路配置如外电阻、极化动力学系数、输入电压的关系也被模拟计算所揭示, 展现出了瞬态负电容效应的丰富可调控策略. 这些结果为实验上合理而高效地利用和设计负电容相关功能电子器件提供了理论参考.